Organic Photovoltaic Modules with New World Record Efficiencies

Dr. Andreas Distler [1], *Prof. Christoph J. Brabec* [1,2,3], *Dr. Hans-Joachim Egelhaaf* [1,2]

1 Solar Factory of the Future, Bavarian Center for Applied Energy Research (ZAE Bayern), Fürther Straße 250, D-90429 Nürnberg, Germany

2 Institute of Materials for Electronics and Energy Technology (i-MEET), Friedrich-Alexander University Erlangen-Nürnberg (FAU), Martensstraße 7, D-91058 Erlangen, Germany

3 Helmholtz Institute Erlangen-Nürnberg for Renewable Energy (HIERN), Immerwahrstraße 2, D-91058 Erlangen, Germany

Keywords: organic photovoltaics (OPV), solar modules, world record, certified power conversion efficiency (PCE), laser patterning

Abstract

During the last years, the development of new active materials has led to constant improvement in the power conversion efficiency (PCE) of solution-processed organic photovoltaics (OPV) to nowadays record values above 17% on small lab cells. In this work, we show the developments and results of a successful upscaling of such highly efficient OPV systems to the module level on large areas, which yielded two new certified world record efficiencies, namely 12.6% on a module area of 26 cm² and 11.7% on a module area of 204 cm².

The decisive developments leading to this achievement include the optimization of the module layout as well as the high-resolution short-pulse (nanosecond) laser structuring processes involved in the manufacturing of such modules. By minimizing the inactive areas within the total module area that are used for interconnecting the individual solar cells of the module in series, geometric fill factors of over 95% have been achieved. A production yield of 100% working modules during the manufacturing of these modules and an extremely narrow distribution of the final PCE values underline the excellent process control and reproducibility of the results.

The new developments and their implementation into the production process of the record OPV modules are described in detail, along with the challenges that arose during this development. Finally, dark lock-in thermography (DLIT), electroluminescence (EL), and photoluminescence (PL) measurements of the record module are presented.

1. INTRODUCTION

Owing to the advent of non-fullerene acceptors, the efficiencies of polymer based organic photovoltaics (OPV) have made a big leap forward in the last three years, after they had stagnated at around 10% in the seven lean years before 2018.[1] A series of publications has recently appeared, demonstrating solution-processed organic solar cells with efficiencies beyond 15%.[2,3,4,5] The present certified record for small area lab cells is at 17.35% efficiency on 0.032 cm².[6] Also, stabilities have reached a reasonable level, with lifetimes of several thousand hours being reported for accelerated ageing tests.[7,8] What is lacking for commercialization of OPV is the upscaling of lab cells to large-area modules. The world record for large-area OPV modules so far has been held by Toshiba, reaching 9.7% on 26.14 cm².[9] The challenges with upscaling are mainly connected to high-quality large-area coating with industrially viable methods and interconnecting cells to modules without losing too much efficiency. The efficiency losses consist of two contributions. On one hand, there are the theoretical losses which arise mainly from the dead area caused by the interconnects and the serial resistances of the electrodes.[10] These losses are intrinsic to the module layout and the materials employed for the electrodes. In the past, we have already presented a study on how to minimize the gap between the efficiencies of small lab cells and large-area modules by numerical optimization of the module layout.[11,12]

On the other hand, there are the losses caused by imperfections of the manufacturing process, such as coating defects and defects caused by inaccurate laser patterning. As the reduction of losses due to series resistance may limit the cell widths to 4 mm or less, minimizing the dead area to less than 5% of the module area requires interconnect widths of max. 200 µm, which in turn requires patterning with resolutions in the 20 µm range.[13] In order to reach these targets and simultaneously achieve high production yields at reasonably high throughput, accurate and reliable laser patterning is essential.

In this paper, we present large-area OPV modules, based on the material system PM6:Y6:$PC_{60}BM$ (see "2. EXPERIMENTAL DETAILS" for full names) with certified world record efficiencies of 12.6% and 11.7%, for module areas of 26.2 cm² and 204.0 cm², respectively. It is described in detail how efficiency losses due to interconnection of cells to modules can be minimized by optimizing laser ablation. This concerns not only the precision in lateral but also in vertical direction, i.e., the high selectivity of layer ablation required to avoid unintentional damage to layers underneath the targeted one. It is shown how important it is to understand the specific challenges of laser patterning. We will also demonstrate that the required quality of laser patterning can be achieved with ns-lasers, rather than requiring fs-lasers, thus reducing the capex for production equipment by an order of magnitude.[14]

2. EXPERIMENTAL DETAILS

An inverted architecture was chosen for all photovoltaic devices in this work. The layer stack is glass/ITO/ZnO/PM6:Y6:$PC_{60}BM$/MoO_x/Ag. Indium tin oxide (ITO) coated glass substrates with a sheet resistance of 15 Ω/□ were purchased from VisionTek. Zinc oxide (ZnO) nanoparticles (2.5wt% in isopropanol) were purchased from Avantama. Poly[(2,6-(4,8-bis(5-(2-ethylhexyl-3-fluoro)thiophen-2-yl)-benzo[1,2-b:4,5-b']dithiophene))-alt-(5,5-(1',3'-di-2-thienyl-5',7'-bis(2-ethylhexyl)benzo[1',2'-c:4',5'-c']dithiophene-4,8-dione)] (PBDB-T-2F, a.k.a. "PM6") and (2,2'-((2*Z*,2'*Z*)-((12,13-bis(2-ethylhexyl)-3,9-diundecyl-12,13-dihydro-[1,2,5]thiadiazolo[3,4-*e*]thieno[2'',3'':4',5']thieno[2',3':4,5]pyrrolo[3,2-*g*]thieno[2',3':4,5]thieno[3,2-*b*]indole-2,10-diyl)bis(methanylylidene))-bis(5,6-difluoro-3-oxo-2,3-dihydro-1*H*-indene-2,1-diylidene))dimalononitrile) ("Y6") were purchased from Derthon OPV. [6,6]-phenyl-C_{61}-butyric acid methyl ester ($PC_{60}BM$) was purchased from Solenne. Molybdenum trioxide (MoO_3) was purchased from Sigma-Aldrich. Silver (Ag) was purchased from Evochem.

The laser patterning of the solar modules, "P1", "P2a/b", and "P3", is conducted by means of a NANIO AIR laser by InnoLas Photonics (P_{max} = 10 W, λ = 532 nm, Nd:YVO_4) with 20 ns pulse width in combination with a galvanometer scanner with f-theta lens and a focal length of 506 mm. The module manufacturing process is described in the following:

Glass/ITO substrates are “P1” laser patterned, followed by a cleaning step with a microfiber tissue and toluene. ZnO nanoparticles are coated with a doctor blade and annealed for 30 min at 200 °C in ambient atmosphere, followed by the “P2a” laser patterning step. PM6:Y6:$PC_{60}BM$ (1:1.1:0.1, 20 mg/ml in chloroform) is stirred at room temperature over night before being coated with a doctor blade using the following processing parameters: 60 µl of solution (stirred at room temperature) are injected into a 400 µm gap between substrate and blade (both heated to 30 °C). Coating with 5-7 mm/s forms a wet film that dries very fast (2-3 s) due to the low boiling point of chloroform (61 °C). Note: this fast evaporation seems to be essential for PM6:Y6:$PC_{60}BM$ when being doctor bladed, since we found that the addition of only 0.5vol% of the high-boiling additive 1-chloronaphthalene to the solution significantly reduces the performance, while it slightly improves the performance when using the spin-coating technique.[3] The devices are subsequently annealed for 10 min at 110 °C under inert atmosphere. The active layer thickness was measured to range between 100-110 nm. Subsequently, 10 nm MoO_x are thermally evaporated, followed by the “P2b” laser patterning step. Finally, 100 nm Ag are thermally evaporated, followed by the “P3” laser patterning step.

Current-voltage characteristics of all modules were recorded with a precision source measurement unit (B2901A by Keysight) under illumination by a class AAA solar simulator (LOT) providing an AM1.5G spectrum at 1000 W/m².

For electroluminescence (EL) and photoluminescence (PL) imaging a Ninox VIS-SWIR 640 camera from Raptor Photonics (Milbrook, Northern Ireland) was used. The camera is equipped with an air-cooled extended Indium-Gallium-Arsenide detector (InGaAs) which is sensitive between 0.4 and 1.7 µm. The camera was controlled using the open source software “Micro-Manager”.[15] Excitation for EL Imaging was carried out with a Keysight B2901A Precision Source/Measure Unit from Keysight Technologies, Inc. (Santa Rosa, California, United States). EL Images were measured with an integration time of 100 ms and corrected for the background. Excitation for PL Imaging was provided by an RLTMGL-532-2.5W 532 nm fiber coupled laser diode (ROITHNER LASERTECHNIK GmbH) with a maximum output power of 2.5W. An integration time of 50 ms was used for recording the PL images. To account for typical deviations in illumination intensity (± 10%), a flat-field correction was performed.

For the dark lock-in thermography (DLIT) measurements an Equus 327k NM infrared (IR)-camera (IRCAM GmbH, Erlangen, Germany) controlled by a computer for real-time lock-in calculations was used. The IR camera is equipped with a cooled indium-antimonite (InSb) and a focal plane array detector (640 x 512 pixels) with a noise equivalent temperature difference less than 20 mK. The IR detector is highly responsive in the spectral range between 1.5–5 µm and provides a frame rate of 100 Hz. The camera was equipped with a 25 mm focal lens imaging system featuring a spectral transparency >90% (IRCAM GmbH, Erlangen, Germany). For all measurements the lock-in frequency was set to 10 Hz in order to minimize implications due to the heat diffusion length. As power supply for the pulsed excitation a source measure unit made by Agilent (B2900) was used.

Details on the calibrated measurements under standard test conditions by the independent certification laboratory of Fraunhofer ISE (Freiburg) can be found as Supporting Information, including the certified current-voltage measurements of the 26 cm² and 204 cm² modules.

3. RESULTS

3.1. Module Optimization

A photovoltaic module generally consists of several solar cells connected in series, which requires distinct patterns of the different layers in the stack. The bottom electrode (e.g., ITO) needs to be patterned in such way that the individual bottom electrodes of all cells of the module are electrically disconnected from each other. The same applies for the top electrode (e.g., Ag). Furthermore, interconnection of all cells in series requires distinct areas between the individual cells, in which the bottom electrode of one cell is brought into direct contact with the top electrode of an adjacent cell with no other layers being present in between. Thus, also the whole layer stack between the bottom and the top electrode needs to feature a specific pattern.

These patterns can be achieved by different means during the production process. On one hand, all layers, including both electrodes, can be deposited directly in the desired pattern with appropriate coating techniques such as inkjet printing, slot die coating of stripes, or thermal evaporation through a mask. On the other hand, all layers can be coated over the full area of the module followed by a patterning step that removes parts of the layers to yield the desired pattern. The respective patterning steps are then called “P1” for the bottom electrode, “P2” for the layer stack between the electrodes, and “P3” for the top electrode. In this work, we pursue the second approach combining full area coating with subsequent patterning steps by means of a pulsed nanosecond(ns)-laser (λ = 532 nm).

Firstly, the ablation thresholds of the different layers are determined by means of single-pulse ablation experiments, in order to establish adequate laser parameters for each patterning process. **Figure 1** summarizes these experiments by showing bright-field (top) and dark-field (bottom) microscope images of the ablation results of the different layer stacks being lasered with varying laser power. The laser ablation is performed in vertical lines with no pulse overlap (single dots). Each vertical line is lasered with a different laser power increasing from left to right within every image, which is indicated by the respective energy values (in µJ) per laser pulse in the top and bottom.

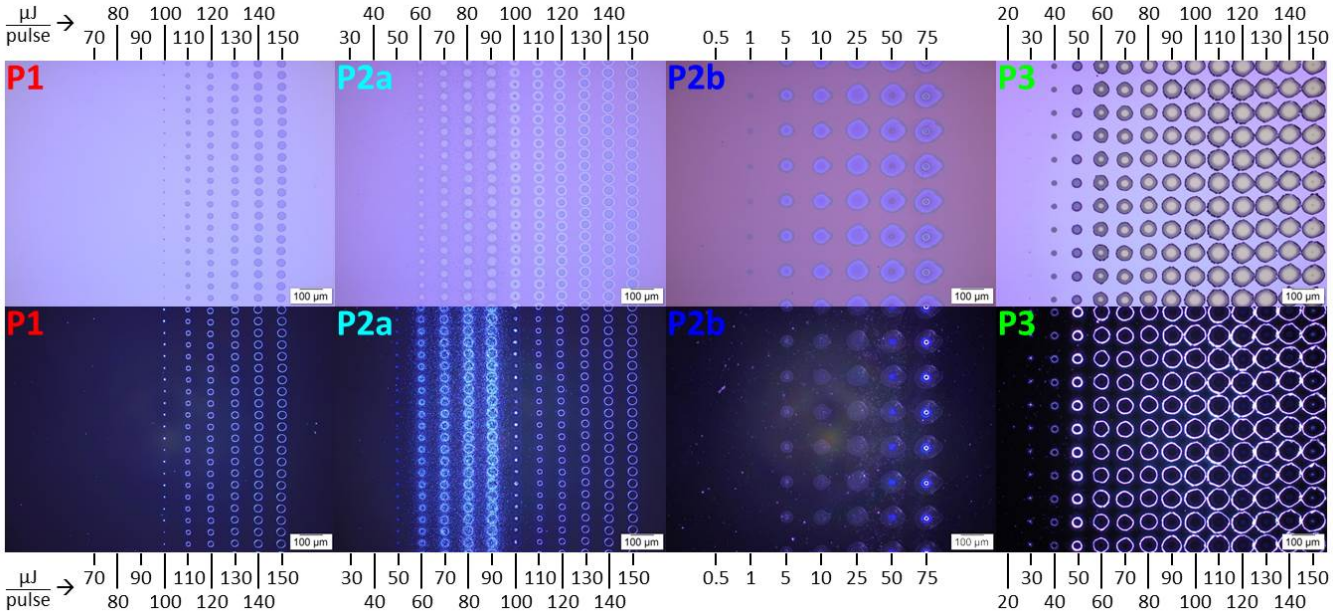

Figure 1: Microscope images (top: bright-field, bottom: dark-field) of single-pulse laser ablations with varying laser power (0.5-150 µJ/pulse) by means of a ns-laser (λ=532 nm) for four different layer stacks: glass/ITO (“P1”), glass/ITO/ZnO (“P2a”), glass/ITO/ZnO/PM6:Y6:$PC_{60}BM$/MoO_x (“P2b”), and glass/ITO/ZnO/PM6:Y6:$PC_{60}BM$/MoO_x/Ag (“P3”).

The two images on the very left-hand side ("P1") show the ablation of an ITO layer on glass. Up to a pulse energy of 90 µJ, the ITO is not visibly damaged. Starting from 100 µJ, ITO ablation can be observed, which becomes more and more pronounced and larger in diameter with further increasing pulse energies.

The two images on the very right-hand side ("P3") show the ablation behavior of the full layer stack (i.e., glass/ITO/ZnO/PM6:Y6:$PC_{60}BM$/MoO_x/Ag. Starting from 30 µJ, one can observe slight damaging of the silver top electrode. At 40 and 50 µJ, the Ag layer is fully ablated, while the active layer underneath remains still present (blue color in bright-field image). Starting from 60 µJ, also the active layer starts to become ablated uncovering the ZnO (beige color in bright-field image). From 100 to 140 µJ, the dark-field microscope images reveal a gradually increasing damaging of ZnO (formation of a blueish center). Eventually, at 150 µJ one observes damaging of the ITO in the very center of each ablation dot.

For the layer stack up to the HTL (i.e., glass/ITO/ZnO/PM6:Y6:$PC_{60}BM$/MoO_x) the ablation results are shown in the middle-right two images ("P2b"). Remarkably, the active layer already starts to get damaged at pulse energies of 1 µJ (discoloration in bright-field image). Between 5 and 25 µJ, the active layer gets fully ablated and the ZnO becomes uncovered but not damaged. At 50 µJ, ZnO starts to get damaged (blue center in dark-field image) but is still not fully ablated (not beige color in bright-field image). Finally, at 75 µJ, ZnO is ablated, but at the same time ITO already gets damaged (blue and white circles in the bright- and dark-field images, respectively).

The latter phenomenon has important implications on the P2 patterning of modules. On one hand, the P2 laser power needs to be strong enough to ablate the whole layer stack, including ZnO, and, by this, uncover the ITO underneath. On the other hand, the laser power must not be too high, because ITO is supposed to remain intact, in order to yield an uncovered ITO area being as big as possible that can form a good interconnect with the top electrode. This implies that the process window for P2 is relatively narrow.

Furthermore, a second, even more severe problem arises for the P2 laser patterning of larger modules using a galvanometer scanner, due to the fact that the angle of incidence of the laser beam onto the module surface is only 0° in the center of the module, but increases towards the outside (e.g., for our setup, ~5° in the corner of a 204 cm^2 module, i.e. 10 cm distance to the center). Since the laser power needs to be as high as 75 µJ/pulse in order to ablate the ZnO layer, the corresponding energy content of the laser beam portion that is reflected at the backside of the 1 mm thick glass substrate of the module is sufficient to destroy the active layer, which is already damaged at 1 µJ/pulse (see cross-section scheme in **Figure 2**). Consequently, for high angles of incidence of the laser beam, the back-reflection beam strikes the active layer again with a large offset to the original position of incidence and, by this, causes "ablation satellites" next to the primary P2 ablation (see microscope images in Figure 2). These satellites would, in our case, lie beyond the adjacent P1/P3 lines of 80 µm distance (i.e., within the active area) for modules broader than ~8 cm.

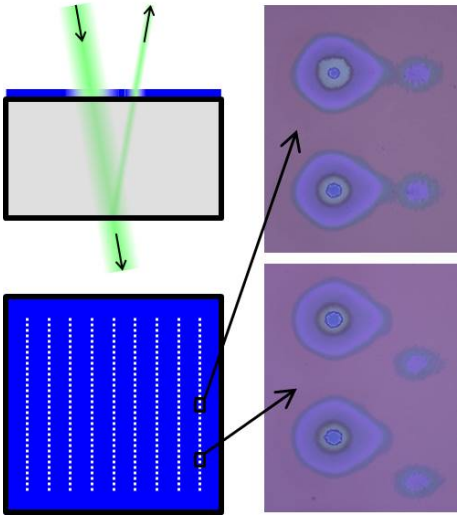

Figure 2: Top left: cross-section of a 1.1 mm glass/ITO substrate coated with the layer stack ZnO/PM6:Y6:$PC_{60}BM$/MoO_x. The green line represents an incident laser beam ablating the whole layer stack (P2) and being partially reflected at the backside of the glass substrate. Bottom left: top view of the substrate with dotted P2 laser lines. Right: bright-field microscope images of such P2 laser dots (75 µJ/pulse) in the middle-right and bottom-right of the module area featuring "ablation satellites" due to back-reflection of the laser.

This is the reason, why ZnO has to be removed before the active layer is applied. Therefore, we subdivide the P2 laser patterning into two separate steps, one of them ("P2a") ablating only the electron transport layer (ETL: ZnO) with high pulse energies directly after it has been coated, and the second one ("P2b") ablating the active layer (AL: PM6:Y6:$PC_{60}BM$) together with the hole transport layer (HTL: MoO_x) with low pulse energies after the latter is coated.

Consequently, we also performed single-pulse ablation experiments on glass/ITO/ZnO samples, in order to obtain adequate laser parameters for the ZnO ablation in the P2a patterning process. The results can be seen in the middle-left two images of Figure 1 ("P2a"). At a laser power of 50 µJ per pulse, the ZnO layer is slightly damaged (see blue dots in dark-field image) but still not fully ablated. From 60 to 90 µJ, ZnO is ablated and the ITO underneath uncovered but fully intact (beige color in bright-field image). Remarkably, a lot of debris is created along the laser line under these conditions, which is shining brightly in the dark-field microscope image. At 100 µJ, ITO starts to get damaged as well (blue center in each ablation dot in the bright-field image), which leads for further increasing laser power to a decrease of uncovered ITO area (beige circles) being available to be contacted by the top electrode to establish the cell interconnect. Astonishingly, as soon as the ITO is slightly damaged (>100 µJ/pulse), the formation of ZnO debris is instantaneously inhibited and no shining areas are observed along the laser lines in the dark-field microscope images.

As elaborated before, the module fabrication process comprises a total of four laser patterning steps, which are alternated by a total of four coating steps (not counting the ITO coating on glass). The whole process is depicted in **Figure 3** including microscope images of the laser lines after each of the four patterning steps. The laser pulse energies that are used for the different patterning steps are chosen based on the previously determined single-pulse ablation thresholds and combined with an optimum pulse-to-pulse distance to yield the desired laser lines. The respective values are 100 µJ / 18.75 µm for P1, 100 µJ / 31.25 µm for P2a, 10 µJ / 31.25 µm for P2b, and 40 µJ / 35 µm for P3. A detailed summary of all laser parameters can be found in **Table 1**.

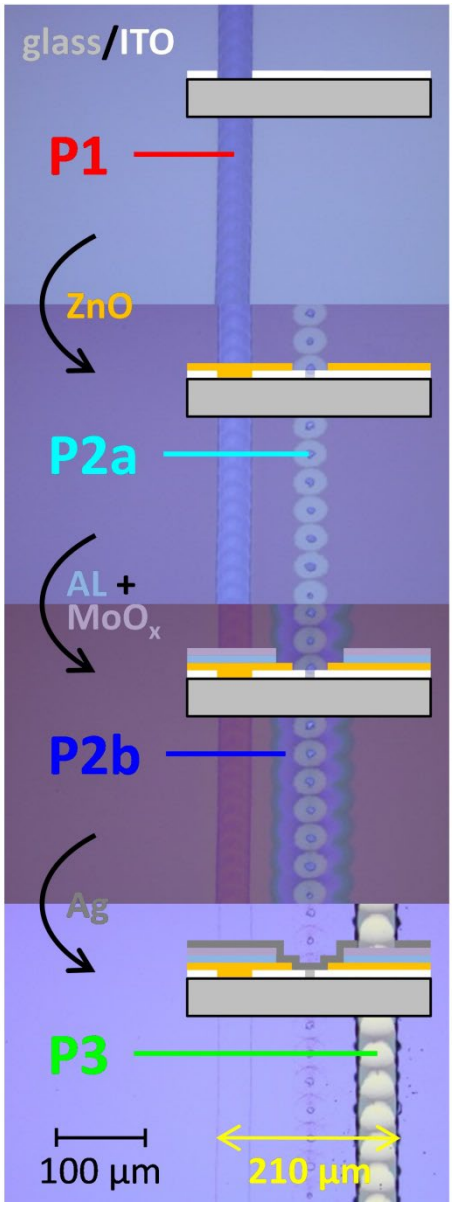

Figure 3: Bright-field microscope images of all laser lines involved in the module production process, namely P1, P2a, P2b, and P3, together with cross-section sketches of the layer stack after each laser patterning step. The black arrows indicate the different coating steps, i.e. electron transport layer (ZnO), active layer (AL: PM6:Y6:$PC_{60}BM$), hole transport layer (MoO_x), and top electrode (Ag).

The distance between P1 and P2a/b as well as between P2a/b and P3 is set to 80 µm, which results in a distance of 210 µm between the left edge of the P1-line and the right edge of the P3-line (see bottom of Figure 3). The area in between, the so called “interconnect area”, is inactive module area, i.e. it does not contribute to the electric power generation of the module. Therefore, it is favorable to minimize this area/distance in order to maximize the active area of the module with respect to its total area. The corresponding ratio is called geometric fill factor (GFF = active module area / total module area). While it is generally possible to further reduce the P1-P2 and P2-P3 distance from 80 µm down to a minimum of 40 µm in order to achieve even higher GFF values, this increases the risk of misalignment during the different laser steps of the manufacturing process and thereby decreases the yield of working modules.

The more cells a module comprises on a given area, the more interconnects (number of cells – 1) lie within the total area of the module, which leads to reduced GFF values and, by this, reduces the overall module efficiency. On the other hand, decreasing the number of cells in a module of given area leads to an increase in cell width, which increases the current flux throughout the module, leading, in turn, to series resistance losses due to the limited conductance of the electrodes (especially ITO) and/or the contact areas interconnecting top and bottom electrodes

(P2). Consequently, there is an optimum number of cells a photovoltaic module should comprise on a given area to yield the maximum GFF without causing additional power conversion efficiency (PCE) losses with respect to the active area of the module. This optimum layout can be simulated as described by Lucera *et al*.[11]

For the materials used in the present work and an interconnect width of 210 µm, an optimum active cell width of 4.1 mm has been calculated and experimentally confirmed for 5.1 cm x 5.1 cm modules (**Figure 4**). It is shown that increasing the active cell width from 2.3 to 4.1 mm does not affect the PCE with respect to the active area of the module (red data), whereas the PCE of the module with respect to its total area (blue data) increases due to the increase of the GFF from 92% to 95%. Increasing the active cell width even further to 4.8 mm does, however, negatively influence the PCE on the active area due to the abovementioned increase of series resistance, which cannot be compensated by the slight increase in GFF from 95% to 96% and, thus, eventually leads to an overall decrease in PCE with respect to the total area of the module.

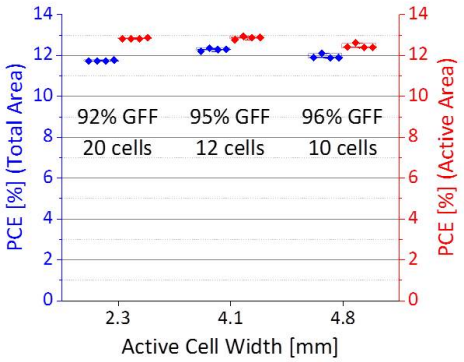

Figure 4: Power-conversion efficiencies (PCE) with respect to the total area (blue data, left y-axis) and the active area (red data, right axis) of modules comprising three different layouts (four modules each layout). The layout variation consists in different cell widths (see x-axis), a different number of cells connected in series, and different geometric fill factors (GFF). The total area of all modules is 26.2 cm².

For single solar cells of inverted architecture with evaporated MoO_x as HTL, the top electrode (e.g. Ag) is usually evaporated right after the MoO_x in one combined evaporation step. However, this is found not to be possible on the module level without causing severe performance losses. In **Figure 5**, the current-voltage characteristics of two mini-modules (0.6 cm², three cells in series) are compared, one of them being P2-lasered after the active layer deposition followed by a combined evaporation of MoO_x and Ag (red), while the other one is P2-lasered between the two evaporation processes, i.e. after the MoO_x deposition (blue). In the case of P2 being patterned before the MoO_x evaporation, one can clearly see that the presence of MoO_x between ITO and Ag in the interconnect area leads to an increased series resistance, which negatively affects the fill factor and leads to a decreased PCE of the module.

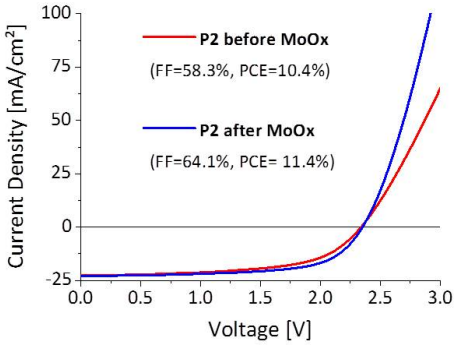

Figure 5: Current-voltage curves of mini-modules (0.6 cm², three cells in series) with P2 being laser-patterned before (red) or after (blue) evaporation of 10 nm MoO_x as hole-transport layer.

3.2. Module Fabrication

Based on all aforementioned optimizations, modules of two different sizes are manufactured in four independent production runs (two for each module size). On one hand, twelve small modules (5.1 cm x 5.1 cm) with 12 cells connected in series and a total module area of 26.2 cm² (active area = 25.0 cm²). On the other hand, six big modules (14.3 cm x 14.3 cm) with 33 cells connected in series and a total module area of 204.0 cm² (active area = 194.8 cm²). In both cases, the total module area is defined by a black mask.

Table 2 summarizes the current-voltage measurements of all manufactured modules, providing on one hand the mean values and standard deviations of the measurements performed in-house (regular) together with the values of the best performing module among these (bold). In addition, the respective values of a certified calibrated measurement under standard test conditions performed by the independent certification laboratory of the Fraunhofer Institute for Solar Energy Systems (ISE) are given in combination with the expanded measurement uncertainties (italic). The corresponding certificates can be found in the Supporting Information.

Remarkably, the manufacturing process exhibits a 100% yield of working modules with an excellent reproducibility, since all twelve small modules show PCE values >12.0% and all six big modules show PCE values >11.7%. Moreover, it is to note that there is only a very minor discrepancy between the values measured in-house and the corresponding certified measurements for the small modules, while this mismatch is a bit more pronounced for the big modules, which could be due to inhomogeneity of the temperature control and/or the illumination intensity over this large area in case of the in-house measurements.

For the best small module, a PCE value of 13.27% with respect to the active area is measured in-house, which corresponds to a PCE of 12.67% with respect to the total module area. The corresponding certified value is 12.60% PCE with respect to the total module area. This is, by far, the highest ever certified PCE for an organic photovoltaic module of similar size.[6] This new record efficiency exceeds the previous record (9.7% PCE on 26.14 cm² by Toshiba)[9] by 30 percent.

The best big module shows an in-house measured PCE value of 12.63% with respect to the active area, which corresponds to a PCE of 12.06% with respect to the total module area. The corresponding certified value is 11.73% PCE with respect to the total module area. Also this value is a new record efficiency for organic photovoltaic modules with an area >200 cm² and exceeds the previous one in this category (8.7% PCE on 802 cm² by Toshiba)[9] even by 35 percent.[6,16]

Figure 6 shows different images of the best small module (certified 12.60% PCE on total area). Firstly, on the left-hand side, a photograph of the twelve-cell module is depicted, which shows the intense blue color of the active layer interrupted by eleven white interconnect lines. The active layer, PM6:Y6:$PC_{60}BM$, which was applied by doctor blade coating from top to bottom, is very homogeneous over the whole area with only ~5% thickness gradient from top (thicker) to bottom (thinner) according to spatially resolved UV/vis absorption measurements. In addition, the active layer appears almost defect-free, with the exception of one small defect visible as a white dot in the fifth cell from the left. By performing dark lock-in thermography (DLIT) at 10 V forward bias, this defect is identified as a pinhole causing shunting, indicated by a bright spot in the DLIT image (second from the left). Remarkably, this shunt has no substantial impact on the overall module performance, which suggests that the shunt acts only very locally, i.e. it has a confined influence region, as elaborated in simulations by Fecher *et al*.[17]

The third image shows the result of an electroluminescence (EL) measurement of the module at 9.5 V forward bias and 7 mA injection current. The measured luminescence intensity is slightly higher in the center of the module and decreases towards all edges and corners (~25% less counts in top-left corner). All areas with no active material being present, namely the interconnect lines and the pinhole, appear dark in the EL image. Finally, on the very right-hand side, a photoluminescence (PL) image of the module being excited with a green laser is shown. Interestingly, the upper part of the module shows a slightly lower PL intensity than the lower part, even though the active layer thickness rather decreases from top to bottom. The pinhole appears as a bright spot.

The images presented in Figure 6 confirm that, at the chosen GFF of 95%, laser patterning is sufficiently precise and reproducible not to introduce any defects at the interconnects. They also demonstrate the high quality of the coating process, all of the layers being highly homogeneous and almost free of defects, which suggests that there is not much room for improvement in module performance by further elimination of coating or patterning defects. The only existing defect is a small pinhole in the active layer that is found to cause only very localized shunting without even affecting the module efficiency. This pinhole is sensitively detected by all four techniques, which demonstrates that these non-destructing imaging methods are sufficiently sensitive to detect even smallest defects, which makes them powerful tools for quality control (QC). PL would even be appropriate as in-line QC technique in a roll-to-roll manufacturing process, as it provides information about the quality of coating and laser patterning already before the finalization of the module.

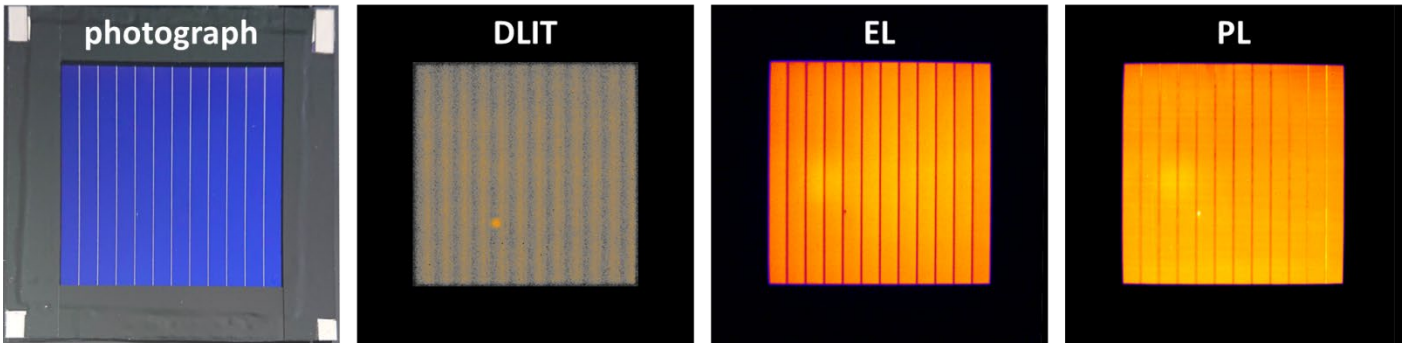

Figure 6: From left to right: a photograph, a dark lock-in thermography (DLIT) image, an electroluminescence (EL) image, and a photoluminescence (PL) image of the best 5.1 cm x 5.1 cm module (certified PCE = 12.6%).

While the focus of this present work was to reproducibly manufacture OPV modules with certified record efficiencies, systematic lifetime studies have not been performed. We ensured however that the modules do not show any significant degradation during our in-house measurements as well as the certification process, which comprises several days and includes irradiation with a full AM1.5G spectrum at 1000 W/m² for a fair amount of time. First results on the stability of PM6:Y6-based devices have been recently reported in the literature, which show T_{80} lifetimes of up to 1000 h under constant illumination.[18,19]

4. CONCLUSIONS

Closing the efficiency gap between lab cells and large-area modules requires both optimization of the module layout and high-quality fabrication methods. We have shown in this paper that the losses due to manufacturing imperfections can be eliminated almost completely by careful design of the manufacturing process. Besides high-quality homogeneous coating of all layers, this requires mainly the accuracy of laser patterning. It has been shown that the main shortcomings comprise in unintentional laser ablation of active layer material within the active area, which leads to local shunting of the device, and the undesired presence of ETL and HTL material in the P2 line, leading to increased interconnect resistance. We have shown how to avoid these issues by modifying the standard patterning sequence and by carefully tuning the laser ablation parameters. The validity of this approach has been confirmed by manufacturing eighteen solar modules based on the high-efficiency material system PM6:Y6:$PC_{60}BM$ with a 100% yield and power conversion efficiencies of close to 13%, which represent the current world records for OPV modules.

This demonstrates that the record efficiencies recently achieved for solution-processed OPV technology can be transferred to the level of large-area modules, which is a game changer for the commercialization of this technology. Equally important for commercial production is the high reproducibility of the production process with production yields of close to unity. We also have demonstrated that the required selectivity and quality of laser patterning can

be achieved not only with fs-lasers but also with ns-lasers, which significantly reduces the investment cost of this technology. Another important step towards the successful commercialization of OPV, is a fully solution-based production process (including HTL and top electrode), which is essential for low-cost manufacturing. This, however, turns out to be especially challenging for the most recent high-efficiency active material systems,[20,21] which is why it has not been addressed in this work yet but is subject of our current developments.

In conclusion, with the efficiencies of solution-processed OPV technology approaching the 20% line on cell level, large-area modules with efficiencies of more than 16% are well within reach, which will bring OPV in the same league as other thin film technologies.

Acknowledgements

The authors acknowledge the 'Solar Factory of the Future' as part of the Energy Campus Nuremberg (EnCN), which is supported by the Bavarian State Government (FKZ 20.2-3410.5-4-5). C.J.B. gratefully acknowledges funding by the Deutsche Forschungsgemeinschaft (DFG, German Research Foundation) under the project numbers 182849149 – SFB 953 and INST 90/917, INST 90/1093-1. The authors thank André Karl from iMEET (FAU) for his support with the EL and PL measurements.

References

[1] NREL, Best Research-Cell Efficiency Chart (https://www.nrel.gov/pv/cell-efficiency.html).

[22] L. Meng, Y. Zhang, X. Wan, C. Li, X. Zhang, Y. Wang, X. Ke, Z. Xiao, L. Ding, R. Xia, H.-L. Yip, Y. Cao, Y. Chen, *Science* **2018**, *361(6407)*, 1094.

[3] J. Yuan, Y. Zhang, L. Zhou, G. Zhang, H.-L. Yip, T.-K. Lau, X. Lu, C. Zhu, H. Peng, P. A. Johnson, M. Leclerc, Y. Cao, J. Ulanski, Y. Li, Y. Zou, *Joule* **2019**, *3*, 1140.

[4] Y. Cui, H. Yao, J. Zhang, K. Xian, T. Zhang, L. Hong, Y. Wang, Y. Xu, K. Ma, C. An, C. He, Z. Wei, F. Gao, J. Hou, Advanced Materials 2020, 32(19), 1908205.

[5] Q. Liu, Y. Jiang, K. Jin, J. Qin, J. Xu, W. Li, J. Xiong, J. Liu, Z. Xiao, K. Sun, S. Yang, X. Zhang, L. Ding, *Science Bulletin* **2020**, *65(4)*, 272.

[6] M. A. Green, E. D. Dunlop, J. Hohl-Ebinger, M. Yoshita, N. Kopidakis, A. W. Y. Ho-Baillie, *Progress in Photovoltaics: Research and Applications* **2020**, *28*, 3.

[7] X. Du, T. Heumueller, W. Gruber, A. Classen, T. Unruh, N. Li, C. J. Brabec, *Joule* **2019**, *3*, 215.

[8] X. Xu, J. Xiao, G. Zhang, L. Wei, X. Jiao, H.-L. Yip, Y. Cao, *Science Bulletin* **2020**, *65(3)*, 208.

[9] M. A. Green, E. D. Dunlop, D. H. Levi, J. Hohl-Ebinger, M. Yoshita, A. W. Y. Ho-Baillie, *Progress in Photovoltaics: Research and Applications* **2019**, *27*, 565.

[10] L. Lucera, F. Machui, P. Kubis, H.-D. Schmidt, J. Adams, S. Strohm, T. Ahmad, K. Forberich, H.-J. Egelhaaf, C. J. Brabec, *Energy & Environmental Science* **2016**, *9(1)*, 89.

[11] L. Lucera, P. Kubis, F. W. Fecher, C. Bronnbauer, M. Turbiez, K. Forberich, T. Ameri, H.-J. Egelhaaf, C. J. Brabec, *Energy Technology* **2015**, *3(4)*, 373.

[12] L. Lucera, F. Machui, H.-D. Schmidt, T. Ahmad, P. Kubis, S. Strohm, J. Hepp, A. Vetter, H.-J. Egelhaaf, C. J. Brabec, *Organic Electronics* **2017**, *45*, 209.

[13] P. Kubis, N. Li, T. Stubhan, F. Machui, G. J. Matt, M. M. Voigt, C. J. Brabec, *Progress in Photovoltaics: Research and Applications* **2015**, *23(2)*, 238.

[14] P. Kubis, J. Winter, A. Gavrilova, M. Hennel, S. Schlosser, I. Richter, A. Distler, M. Heyder, S. Kery, P. Lenk, S. Geiger, C. J. Brabec, H. P. Huber, H.-J. Egelhaaf, *Progress in Photovoltaics: Research and Applications* **2019**, *27(6)*, 479.

[15] A. Edelstein, N. Amodaj, K. Hoover, R. Vale, N. Stuurman, Current Protocols in Molecular Biology **2010**, *92(1)*, 14.20.1.

[16] NREL, Champion Photovoltaic Module Efficiency Chart (https://www.nrel.gov/pv/module-efficiency.html).

[17] F. Fecher, A. Peréz Romero, C. J. Brabec, C. Buerhop-Lutz, *Solar Energy* **2014**, *105*, 494.

[18] S. Li, C.-Z. Li, M. Shi, H. Chen, *ACS Energy Letters* **2020**, *5*, 1554.

[19] G. Zhang, X.-K. Chen, J. Xiao, P. C. Y. Chow, M. Ren, G. Kupgan, X. Jiao, C. C. S. Chan, X. Du, R. Xia, Z. Chen, J. Yuan, Y. Zhang, S. Zhang, Y. Liu, Y. Zou, H. Yan, K. S. Wong, V. Coropceanu, N. Li, C. J. Brabec, J.-L. Bredas, H.-L. Yip & Y. Cao, *Nature Communications* **2020**, *11*, 3943.

[20] Lulu Sun, Wenwu Zeng, Cong Xie, Lin Hu, Xinyun Dong, Fei Qin, Wen Wang, Tiefeng Liu, Xueshi Jiang, Youyu Jiang, Yinhua Zhou, *Advanced Materials* **2020**, *32(14)*, 1907840.

[21] Y. W. Han, S. J. Jeon, H. S. Lee, H. Park, K. S. Kim, H.-W. Lee, D. K. Moon, *Advanced Energy Materials* **2020**, *9(42)*, 1902065.

Table 1: Laser parameters for P1, P2a, P2b, and P3 (v: scan speed, ν: pulse frequency, d: pulse-to-pulse distance along the laser line, P: laser power, E: pulse energy):

	Passes	v [mm/s]	ν [kHz]	d [µm]	P [W]	E [µJ]
P1	2x	1500	80	18.75	8	100
P2a	1x	2500	80	31.25	8	100
P2b	1x	2500	80	31.25	0.8	10
P3	1x	3500	100	35	4	40

Table 2: Measured open-circuit voltage (V_{OC}), short-circuit current (I_{SC}), fill factor (FF), maximum power point voltage (V_{MPP}), maximum power point current (I_{MPP}), maximum power output (P_{MPP}), and power conversion efficiency (PCE) with respect to the total/active area of twelve small modules (26.2 cm²) and six big modules (204.0 cm²). Regular: mean values and standard deviations of in-house measurements. **Bold: values of the best module measured in-house.** *Italic: certified values and expanded measurement uncertainties of the best module measured by Fraunhofer ISE.*

Module Area [cm²] (Total / Active)	Cells in Series	V_{OC} [V]	I_{SC} [mA]	FF [%]	V_{MPP} [V]	I_{MPP} [mA]	P_{MPP} [mW]	PCE [%] (Total Area)	PCE [%] (Active Area)
26.2 / 25.0	12	9.798 ± 0.037	45.44 ± 0.42	72.79 ± 0.69	8.100 ± 0.139	40.01 ± 0.73	324.0 ± 4.1	12.37 ± 0.16	12.95 ± 0.16
		9.824	**45.96**	**73.54**	**8.216**	**40.41**	**332.0**	**12.67**	**13.27**
		9.978 ± 0.040	*46.43 ± 0.65*	*71.06 ± 0.38*	*8.230*	*40.00*	*329.2 ± 4.8*	*12.60 ± 0.19*	*13.19 ± 0.20*
204.0 / 194.8	33	26.77 ± 0.14	130.4 ± 2.2	69.37 ± 0.50	20.87 ± 0.08	116.2 ± 1.5	2424 ± 27	11.89 ± 0.13	12.45 ± 0.14
		26.74	**133.3**	**69.02**	**20.90**	**117.7**	**2460**	**12.06**	**12.63**
		26.99 ± 0.11	*127.9 ± 1.8*	*69.35 ± 0.37*	*21.96*	*108.9*	*2393 ± 35*	*11.73 ± 0.17*	*12.28 ± 0.18*